Influence of grain structure and slip planarity on fatigue crack growth in low alloying artificially aged 2xxx aluminium alloys

N. Kamp[a,b], N.Gao[a], M.J. Starink[a], I. Sinclair[a,*]

[a] *Materials Research Group, School of Engineering Sciences, University of Southampton, UK*

[b] *Currently at School of Materials, University of Manchester, UK*

[*] Corresponding author. School of Engineering Sciences, Southampton University, UK, i.sinclair@soton.ac.uk (I. Sinclair)

keywords: fatigue crack growth, slip bands, grain structure, crack closure, 2xxx aluminium alloys

Abstract

The fatigue crack growth behaviour under constant amplitude loading of three low alloying artificially aged 2xxx aluminium alloys with distinct microstructures is analysed. Fatigue crack growth tests show a correlation between fatigue performance and the occurrence of crack closure. Fractography and fracture surface measurements show that rougher surfaces give higher closure levels suggesting a dominating influence of roughness induced crack closure in these alloys. The relationship between the crack path and the microstructure, i.e. grain structure and slip planarity, is assessed semi-quantitatively. A criterion to evaluate the propensity for slip band formation is derived and reasonable correlation is found between the fatigue fracture behaviour of the three alloys and this criterion.

1. Introduction

Recent developments in the age-forming process where a curved component is formed using a combination of pressure and temperature have highlighted the need for heat treatable 2xxx aluminium alloys retaining strength and damage tolerant properties similar to the incumbent 2024-T351 and related variants [1,2]. However, in 2xxx aluminium alloys, fatigue crack propagation resistance is known to decrease with significant artificial ageing [3]. The specific fatigue behaviour of low solute, artificially aged 2xxx alloys is largely unknown whereas the fatigue behaviour of naturally aged 2xxx aluminium alloys has been extensively studied (see e.g. [4]). It is therefore highly valuable to assess and review the fatigue behaviour of these alloys in light of known fatigue crack propagation mechanisms occurring in aluminium alloys. Microstructural effects have a strong influence on fatigue crack growth rates near threshold. Suresh *et al*. [4] have highlighted the influence of the grain structure and slip characteristics in aluminium alloys. The occurrence of persistent slip band (PSB) is beneficial to the fatigue crack growth properties via intrinsic and extrinsic mechanisms. Intrinsically, during fatigue crack growth the kinematical reversibility of cyclic slip may be enhanced by the PSB reducing damage accumulation [4]. Extrinsically, PSBs may promote crack deflection along a favoured slip system which leads to a more tortuous crack path and may contribute to the occurrence of roughness induced crack closure (RICC). Although other crack closure mechanisms are known to occur, such as plastically induced crack closure (PICC), for near-threshold conditions with a small active plastic zone size compared to the size of shear displacements inducing RICC, RICC may be considered as the dominant crack closure mechanism. As such, in the following, crack closure is discussed considering

the influence of PSB contributing mainly to RICC although it is acknowledged that PICC may also play a role.

Precipitation-hardened 2xxx aluminium alloys are used in underaged condition where the strengthening precipitates are shearable and may therefore prompt the formation of slip bands. Grain boundaries act as barriers to PSB and subsequently the grain size can be taken as a measure of crack deflection, i.e. larger grain size gives longer deflections. However, studies have shown that texture is also an important parameter [5] as deflected cracks have been shown to propagate across several grains particularly across low angle grain boundaries. The analysis of these microstructural influences is also convoluted, in mode I loading, to the crack natural propensity to propagate perpendicular to the loading direction (direction of maximum tensile opening and strain energy release rate).

The influence of these microstructural parameters on fatigue crack growth is discussed in this paper for three low solute artificially aged Al-Cu-Mg-(Mn,Zr,Sc)-(Li) alloys with distinct microstructural features.

2. Materials and heat treatments

Three Al-Cu-Mg-X alloy plates, of 150x20mm cross section, were rolled by QinetiQ plc, Farnborough UK, compositions are shown in Table 1. In particular the alloys cover variations in Li content and dispersoid type. All three alloys have similar Cu/Mg ratios, whilst Alloys 1 and 2 have a higher Li content compared to Alloy 3. Dispersoids are Zr-containing in Alloy 1, Mn-containing in Alloy 2, whilst Alloy 3 has both Zr- and Sc-containing dispersoids.

The plates were supplied in solutionised, quenched and stretched condition. For the present study, all alloys were artificially aged at 190ºC for 12 hours, whilst Alloy 1 was also investigated for an alternative ageing treatment of 150ºC for 12 hours.

3. Experimental

Optical microscopy was performed on these alloys using samples polished and etched using Keller's reagent to reveal the grain structure. Polished samples were also subsequently electropolished to perform electron back scattered diffusion (EBSD) analysis using a JSM-6500 FEG-SEM with HKL Channel 5 software.

Differential scanning calorimetry (DSC) experiments were conducted using a Perkin-Elmer Pyris 1 DSC. Disc-shaped samples with a thickness about 0.9mm and diameter 5mm were used. Experiments were performed at a constant heating rate of 10°C/min.

Tensile tests were carried out according to ASTM E-8 standards [6] for each condition on three similar cylindrical hounsfield specimens with a 25mm gauge length. Specimens were taken in the longitudinal (L) direction. Fatigue crack propagation tests were carried out according to ASTM E-647 standards [7] using compact tension (CT) specimens (of length 32mm and thickness 16mm) taken from the plates mid-thickness in the LT orientation. Tests were conducted in air at room temperature with a loading frequency of 20Hz at a stress ratio (R) of 0.1. Crack closure measurements were obtained using a crack mouth clip gauge set up similar to Xu *et al*. [8] with a loading frequency of 1Hz and closure levels were calculated using a non-subjective curve fitting method described in [8]. SEM fractographic analysis was performed on the failed samples.

4. Results

4.1 Grain structure

Grain structures for the different alloys are shown in Fig. 1 and their respective grain sizes (mean intercepts in the T and S directions) are given in Table 2. EBSD grain structure maps are shown in Fig. 2. Fig. 2 shows that the three alloys have very distinct grain structures: (i) Alloy 1 is partially recrystallised, four types of grains can be observed in this alloy - large unrecrystallised grains, small recrystallised grains, large recrystallised grains, and subgrains (ii) Alloy 2 exhibits a relatively coarse, recrystallised equiaxed grain structure (iii) Alloy 3 is largely unrecrystallised and exhibits a particularly fine grain structure (~10μm) and subgrain structure in the S-direction.

4.2 Strengthening precipitates and tensile properties

The results of the DSC experiments for Alloy 1 aged at 150°C and 190°C for 12h are shown in Fig. 3. The first endothermic peak for the alloy aged at 150°C represents the dissolution of clusters and/or small δ' (Al_3Li) precipitates. This peak is very small for the same alloy aged at 190°C. The first exothermic peak represents the formation of S phase. The second exothermic peak around 380°C is thought to be T_2 (Al_6CuLi_3) formation and the final endothermic peak represents the dissolution of S (Al_2CuMg) and T_2 phases [9]. This suggests that the main strengthening precipitates for Alloy 1 aged at 150°C for 12h are clusters with limited amount of S phase whereas S phase is the main strengthening precipitate when Alloy 1 is aged at 190°C for 12h with a very limited amount of clusters remaining in this condition.

Fig. 4 shows the results of the DSC experiment for Alloys 1, 2 and 3 aged at 190°C for 12h. These curves show mainly or exclusively endothermic effects, indicating that precipitation is nearly complete. DSC curves for Alloys 1 and 2 are relatively similar.

Alloy 3 has no precipitates formation peak. This suggests that after 12h ageing at 190°C all precipitates have formed in this alloy, ie. the alloy is in overaged condition. Dissolution in this alloy starts around 220°C up to 500°C, the first part of the peak is associated with dissolution of clusters and becomes gradually associated with S phase dissolution. Alloy 3 is therefore deduced to contain both clusters and S phase. A summary of the alloy microstructural properties is presented in Table 3.

Tensile properties for the alloys considered are given in Table 4. Alloy 1, 2 and 3 aged at 190°C for 12h have similar tensile properties in terms of yield strength (YS), ultimate tensile strength (UTS) and elongation with Alloy 2 being marginally weaker than the other two. Alloy 1 aged at 150°C for 12h has a lower YS but similar UTS, whilst its elongation is also significantly higher.

4.3 Fatigue crack growth

da/dN vs. ΔK results for the Alloy 1 aged at 150°C and 190°C for 12h are shown in Fig. 5. In Fig. 5 and 6, a relatively large scatter for 2024-T351 plate fatigue crack growth rates, taken from available literature data [10] for centre cracked tension panels specimens, is given for comparison. As expected, the more underaged alloy performs better. Alloy 1 aged at 150°C for 12h has a slower fatigue crack growth rate than 2024-T351. Alloy 1 aged at 190°C for 12h has a fatigue crack growth rate close to the lower bound of the 2024-T351 alloy scatter band at intermediate ΔK and has a higher ΔK at near-threshold, which will be noted thereafter ΔK_{th} (it should be noted that in this study near-threshold was assumed for da/dN<10^{-6} mm/cycle).

da/dN vs. ΔK results for Alloys 1, 2 and 3 aged at 190°C for 12h are shown in Fig. 6. Alloy 2 exhibits relatively good fatigue performance while Alloy 3 fatigue properties are worse than 2024-T351 at intermediate ΔK and just fall within the 2024-T351

scatter band at lower and higher ΔK. Alloy 2 has large, recrystallised grains compared to Alloys 1 and 3 which have an unrecrystallised, fine grain structure. As such, large, recrystallised grains are seen to enhance fatigue performance in Alloy 2 compared to Alloys 1 and 3, as previously shown in the literature [11].

Measured crack closure levels as a function of ΔK for the different alloys are given in Fig. 7. Though the difficulty in obtaining exact crack closure measurements is well reported [8,12,13,14], general trends in the sensitivity to crack closure of each alloy tested in the same condition can still be deduced. Fig. 5, 6 and Fig. 7 show that the closure levels (K_{cl}/K_{max}, where K_{cl} is the crack closure stress intensity factor and K_{max} is the stress intensity factor at maximum load) of the different alloys scale with their fatigue performance. Alloy 3 has the lowest closure levels and is associated with the worst fatigue performance. Closure levels for Alloy 1 are aboveAlloy 3 and below Alloy 2 for alloys heat treated at 190°C.

From the fracture surfaces of the failed fatigue specimens, various features can be recognized (Fig. 8-11). All the cracks propagate macroscopically in mode I but are seen to deviate locally. Clear faceting can be observed at low ΔK for Alloy 1 aged at 150°C in Fig. 8. Linear features extending to several hundreds of microns in the crack propagation direction highlight the influence of the underlying grain structure. However the varied surface features suggest the presence of competing mechanisms of the crack propagation. This alloy possesses smoother and rounder features typical of ductile fatigue fracture at higher ΔK. The progressive transition between ductile and crystallographic crack propagation has been observed at intermediate ΔK.

Fatigue fracture surface features at high and low ΔK for Alloys 1, 2 and 3 aged at 190°C for 12h are shown respectively in Fig. 9, 10 and 11. Features for Alloy 1 aged at 190°C at high ΔK in Fig. 9 are similar to Fig. 8. However a higher proportion of

clearly crystallographic features is seen in Alloy 1 aged at 150°C for both low and intermediate Δ*K*. Though the features become more fine scaled and more evidence of interaction of the crack path with grain boundaries was found at low Δ*K* in Alloy 1 aged at 190°C compared to high Δ*K*, no clear faceting was observed. It can be seen from Fig. 10 that at low Δ*K* crack propagation in Alloy 2 is fully crystallographic with again a transition to more ductile fracture features at higher Δ*K*. The intermediate Δ*K* region is shown in Fig. 10b) and exhibits 'herring bone' features. In Fig. 11 a transition between very fine features at low Δ*K* to larger and rounder features at higher Δ*K* can be observed for Alloy 3.

EBSD maps of the crack profile (LT direction) for Alloys 2 and 3 are shown in Fig. 12 and 13. Fig. 12 and 13 clearly illustrate the different scales of the fracture surface features between Alloy 2 and 3 (Alloy 1 being intermediate). Also, no clear interaction behavior of the crack path with the grain boundaries is observed even at low Δ*K*.

5. Discussion

5.1 Crack propagation mode

Crack propagation in 2xxx aluminium alloys tend to evolve from 'ductile' fatigue fracture at high *ΔK* to a more 'crystallographic' path at low Δ*K* [10]. The crack paths in all our alloys and conditions were macroscopically straight. However, clear evidence of microscopically deviated paths was observed in all our alloys, especially at low *ΔK* where rougher more crystallographic crack paths were seen, see Fig. 8-11. Evidence of crystallographic crack propagation was still observed in all these alloys at *ΔK*~7-10MPa√m but less distinctly. A summary of the fatigue fracture surface features is presented in Table 5.

Crack propagation in aluminium alloys is known to depend on a combination of several parameters: (i) state of recrystallisation (ii) grain boundary 'strength' (linked to grain misorientation) (iii) intensity and type of texture (iv) orientation of the specimen (in relation to the grain structure) (v) propensity for slip band formation.

These parameters can be used to explain the differences in crack propagation modes between these alloys:

- Alloy 1 aged at 150°C and 190°C: the same alloy in different ageing conditions exhibits distinct changes in crack propagation behaviour. The main microstructural difference between these two variants of the same alloy lies in the nature of the strengthening precipitates: zones/clusters at 150°C and S phase at 190°C. It therefore confirms that the nature of the strengthening precipitates may affect the propensity for slip formation and in turn influences the crack propagation mode. Slip band formation is greater in the presence of shearable clusters rather than non-shearable S phase.
- Alloy 1 and 2 aged at 190°C: the complex interaction between the above parameters is clearly illustrated by the difference in the crack propagation between these alloys. Alloy 2 crack propagation evolves from fully ductile to fully crystallographic with deflection and facets at low ΔK roughly of the same size order as the equiaxed grain size, whereas features in Alloy 1 are much more varied due to its more varied arrangement of grain structure. Influence of varied grain structure on the crack path is illustrated in Fig. 14 where several possible combinations associated with transgranular crack propagation between adjacent grains depending on their size, recrystallisation state and orientation to the main slip systems are shown.
- Alloy 1 and 3 aged at 190°C: the addition of dispersoids and the refined grain structure in Alloy 3 compared to Alloy 1 does not seem to affect the crack

propagation mode. However, Alloy 3 clearly exhibits much finer fatigue fracture surface features.

The influences of some of the parameters mentioned above may be difficult to estimate, such as the relationship between the crack path and statistical distributions of grain boundary misorientations of the alloy. If the alloy is dominated by a given texture (as opposed to a more random orientation of grain structure), misorientation angles between adjacent grains may be small and a crack may propagate across several grains (misorentation of close packed planes between adjacent planes is small and slip band can propagate across several grains offering a preferential crack path). Fig. 15 shows pole figures of all three alloys considered here. It can be seen that Alloy 1 and 3 have higher texture peak intensities. These results are contrary to the observed faceting in our alloys which is predominant in Alloy 2. This implies that the influence of texture is convoluted in these alloys to the grain size and propensity for slip formation.

5.2 Determination of slip planarity

Comparison between the two ageing conditions of Alloy 1 has shown the influence of the slip planarity as one of the main driving force controlling crack propagation. Models have been proposed in the literature to assess both the influence of the slip bands characteristics on crack propagation [15,16] and a given alloy's propensity for slip band formation [17,18,19]. In order to determine the propensity for slip formation Blankenship *et al*. [19] considered the influence of a combination of shearable and non-shearable precipitates where: (a) slip bands are formed by successive dislocations cutting through shearable precipitates where softening occurs as the effective size of the particles decreased, (b) strong precipitates that are non-shearable when their size

exceed a critical size, with the inter-particle spacing of non-shearable precipitates then determining the effective length of slip bands. The critical particle size depends on the number of dislocations in the pile-up. The deformation behaviour can then be predicted by comparing the predicted particle critical size (d_c) and the measured precipitates size (d), i.e. if $d_c>d$ deformation is planar and if $d_c<d$ deformation is homogeneous. Blankenship *et al*. [19] give the number of dislocation N expected in a pile-up in an alloy strengthened by shearable precipitates [19]:

$$N = \sqrt{V_f}\sqrt{r_p}L\frac{C_p}{C_B b} \qquad \text{(Eq. 1)}$$

where V_f is the volume fraction of shearable precipitates, r_p the shearable particle radius, L is the slip length, b is the burgers vector, C_p is a term related to the antiphase boundary energy (ABE) and C_B is related to the matrix shear modulus. For similar alloy systems and precipitates C_p, C_B and b are assumed to be identical. Therefore, a criterion, N_c, evaluating the propensity for slip formation to compare similar alloy system can be derived as:

$$N_c = \frac{NC_B b}{C_p} = L\sqrt{V_f r_p} \qquad \text{(Eq. 2)}$$

This criterion may help understand and rationalize the materials behavior in view of the microstructural parameters as well as provide a semi-quantitative predictive tool for fatigue crack growth behavior.

Blankenship *et al*. [19] assumed that the slip length L is the spacing between non-shearable S particles. In this study where large variation in the grain structures are

observed, the grain size is considered as the main parameter in determining the slip length and $L=L_{GS}$.

Detailed precipitation studies for Alloy 1 and 2 were performed Gao *et al*. [9] using a combination of DSC, TEM and three dimensional atom probe (3DAP). The average radius of the clusters/δ' precipitates formed after 12h at 150°C was found to be around 2.25nm; a similar radius is assumed for clusters that may remain in the matrix after ageing at 190°C for 12h. S phase present in alloys aged at 190°C for 12h appear as needle shaped particles ~100nm in length and with a 20nm width. The volume fraction of the different precipitates is evaluated by integrating the DSC heat flow over time for the different precipitation and dissolution peaks [20], in a first order approximation a linear relationship is assumed between the total heat evolved and the volume fraction of the different precipitates. Gao *et al*. [9] estimated the volume fraction of δ' precipitates to be 1.32% for Alloy 2 aged at 150°C for 12h from 3DAP experiments (ie. considering a small volume of material). The same volume fraction is assumed for Alloy 1 aged at 150°C for 12h, subsequently all the total heat evolved calculated can be related to precipitates volume fraction. A summary of the alloys microstructural parameters is presented in Table 6. In this study, precipitates precursors (cluster zones) and early precipitates (δ') are assumed to be shearable and favour slip band formation, however clusters strengthen the alloy by modulus hardening which is independent of the cluster size (ie. no softening occurs when clusters are cut by dislocations) rather order strengthening [21,22], as such Eq. 2 can only be applied for these alloys in first approximation to obtain a general trend, noting that local softening may indeed arise from multiple dislocation shear as the clusters within a slip band are either taken below their critical radius for dissolution (e.g. see [23]) or atoms in very small clusters are effectively moved apart by the passage of

dislocations. Eq. 2 parameters and the indicator N_c for the alloys propensity to slip band formation are given in Table 7. The criterion scales with the observed fatigue fracture behaviour. Alloy 2 exhibiting large blocky facets at low ΔK (Fig. 10) and a relatively good fatigue performance has a significantly higher N_c value than the other alloys. Alloy 1 heat treated at 150°C, which has similar fatigue performance compared to Alloy 2 and also exhibits some amounts of block faceting (Fig. 8), has a relatively high N_c value while Alloy 1 aged at 190°C has a comparatively low N_c value and has much less visible crystallographic features on its fatigue fracture surface (Fig. 9) than the two previous alloys. Alloy 3 has a similar N_c value and similar fatigue failure mode compared to Alloy 1 aged at 190°C (see 5.1). Therefore, despite a number of approximations in the determination of the parameters determining N_c, this criterion adequately describe the propensity of an alloy to form slip bands and can be used to predict and compare qualitatively the fatigue failure mode of similar alloys having different compositions and grain sizes.

6. Conclusion

The influence of the microstructure, i.e. grain structure, dispersoids, strengthening precipitates, on the crack propagation of several Al-Cu-Mg-X alloys has been examined. Varying the nature and content of dispersoids achieved distinct grain structures. The fatigue crack growth performance of these alloys has been related to the occurrence of roughness induced crack closure and the crystallographic nature of the crack path at low ΔK. Underaged alloys and alloys with a larger grain size appear to have better overall fatigue crack growth performance. This is particularly relevant in terms of alloy development as it indicates that ageing to peak aged or overaged conditions in this alloy system is detrimental to fatigue crack growth performance

imposing limitation on process temperature/time combinations. Also, Sc-induced grain refinement, which is known to significantly improve both strength and toughness, appears detrimental to fatigue crack growth performance. The transition between ductile crack propagation and crystallographic crack propagation was illustrated for all alloys. Existing models were used to rationalise the fatigue behaviour of these alloys. Reasonably good agreement was found between a criterion evaluating the propensity of each alloy to exhibit slip bands and the experimental observations of the alloys' behaviour.

Acknowledgement

The technical and financial support of the EPSRC, Airbus and QinetiQ plc are gratefully acknowledged.

References

[1] Starink MJ, Sinclair I, Gao N, Kamp N, Gregson PJ, Pitcher PD, Levers A, Gardiner S. Development of new damage tolerant alloys for age-forming Mater Sci Forum 2002:396-402;601-606.

[2] Starink MJ, Gao N, Kamp N, Wang SC, Pitcher PD, Sinclair I. Relations between microstructure, precipitation, age-formability and damage tolerance of Al-Cu-Mg-Li (Mn,Zr,Sc) alloys for age forming Mater. Sci. Eng. A, Vol. 418, 2006, pp 241-249.

[3] Bray GH, Glazov M, Rioja RJ, Li D, Gangloff RP. Effect of artificial aging on the fatigue crack propagation resistance of 2000 series aluminium alloys Int Jnl Fatigue 2001;23:S265-S276.

[4] Suresh S, Vasudevan AK, Bretz PE. Mechanisms of slow fatigue crack-growth in high-strength aluminum alloys - role of microstructure and environment Metall Trans A 1984;15:369-379.

[5] Rao KTV, Ritchie RO. Fatigue of Aluminum-Lithium Alloys. Int Mater Rev 1992;37:153-183.

[6] ASTM standard E 8, Annual book of ASTM Standards, American Society for Testing and Materials, Philadelphia, PA, 1996.

[7] ASTM standard E 647, Annual book of ASTM Standards, American Society for Testing and Materials, Philadelphia, PA, 1996.

[8] Xu Y, Gregson PJ, Sinclair I. Systematic assessment and validation of compliance-based crack closure measurements in fatigue. Mater. Sci. Eng. A 284 2000;284:114-125.

[9] Gao N, Starink MJ, Davin L, Cerezo A, Wang SC, Gregson PJ. Microstructure and precipitation in Al-Li-Cu-Mg-(Mn, Zr) alloys Mater Sci Tech 2005;21:1010-1018.

[10] Xu Y, Gregson PJ, Sinclair I. Dispersoid and grain size effects on fatigue crack growth in AA2024-type alloys Mater Sci Forum 2000;331-7;1525-1530.

[11] Kirby BR, Beevers CJ. Slow fatigue crack growth and threshold behavior in air and vacuum of commercial aluminum alloys Fatigue Eng Mater Struct 1979;1:203.

[12] Schijve J. Fatigue crack closure observations and technical significance. In: *Mechanics of fatigue crack closure. ASTM STP 982*, American Society for Testing and Materials, Philadelphia, PA (1988), pp. 5–34.

[13] Allison JE, Ku RC, Pompetzki MA. A comparison of measurements methods and numerical procedures for the experimental characterization of fatigue crack closure. In: *Mechanics of fatigue crack closure. ASTM STP 982*, American Society for Testing and Materials, Philadelphia, PA (1988), pp. 171-185.

[14] Lee CS, Park CG, Chang YM. Precise determination of fatigue crack closure in Al alloys Mater Sci. Eng A 1996;216:131-138.

[15] Rading GO, Berry JT. On deviated and branched crack path in Al-Li-X alloys Mater Sci Eng A 1996;219:192-201.

[16] Patton G, Rinaldi C, Brechet Y, Lormand G, Fougeres R. Study of fatigue damage in 7010 aluminum alloy Mater Sci Eng A 1998;254:207-218.

[17] Duva JM, Daeubler MA, Starke EAJ, Lutjering G. Large shearable particles lead to coarse slip in particle reinforced alloys Acta Metall 1988;36:585-589.

[18] Blankenship CP, Starke EAJ. Mechanical behavior of double aged AA8090 Metall Trans A 1993;24:833841.

[19] Blankenship CP, Hornbogen E, Starke EA. Predicting slip behavior in alloys containing shearable and strong particles Mater Sci Eng. A 1993;169:33-41.

[20] Starink MJ.The Analysis of Al-Based Alloys by Calorimetry: Quantitative Analysis of Reactions and Reaction Kinetics. Int Mater Rev 2004;49:191-226.

[21] Starink MJ, Wang P, Sinclair I, Gregson PJ. Microstructure and strengthening of Al-Li-Cu-Mg alloys and MMCs: II. Modelling of yield strength Acta Mater 1999;47:3855-3868.

[22] Starink MJ, Gao N, Davin L, Yan J, Cerezo A. Room temperature precipitation in quenched Al-Cu-Mg alloys: a model for the reaction kinetics and yield strength development. Philos Mag A 2005;85:1395-1418.

[23] Brechet Y, Louchet F, Marchionni C, Vergergaugry Jl. Experimental (TEM and STEM) investigation and theoritical approach to the fatigue-induced dissolution of delta' precipitates in a 2.5wt-percent Al-Li alloy. Philos Mag A 1987;56:353-366.

Alloys	Cu	Mg	Li	Zr	Mn	Sc
1	2.27	1.03	1.56	0.106	-	-
2	2.24	0.94	1.60	-	0.42	-
3	2.08	0.97	0.55	0.11	-	0.21

Table 1. Alloy compositions (weight %).

Alloys		1	2	3
Grain size*	S	11	64	5
(μm)	T	18	83	9

* obtained from line intercept measurements

Table 2. Grain sizes.

Alloys	**Grain Structure**	**Solute elements**	**Precipitates**	**Added elements for dispersoid formation**
Alloy 2	Coarse Recrystallised	High Li	Some δ′ + clusters + S phase^{*190}	0.4Mn
Alloy 1	Fine Partially recrystallised	High Li	Some δ′ + clusters^{*150} + S phase^{*190}	0.1Zr
Alloy 3	Very fine Partially recrystallised	Mid Li	clusters + S phase^{*190}	0.1Zr + 0.2Sc

^{*150} and ^{*190} indicates respectively the main strengthening precipitate phase after ageing at 150°C and 190°C

Table 3. Summary of alloy properties. Alloys are ordered according to their general fatigue performance (better fatigue resistance first).

Heat treatment	**150°C/12h**	**190°C/12h**		
Alloys	**1**	**1**	**2**	**3**
Tensile strength (MPa)	400	399	393	397
Yield strength (MPa)	294	365	343	369
Elongation (%)	22	14	13	15

Table 4. Tensile properties.

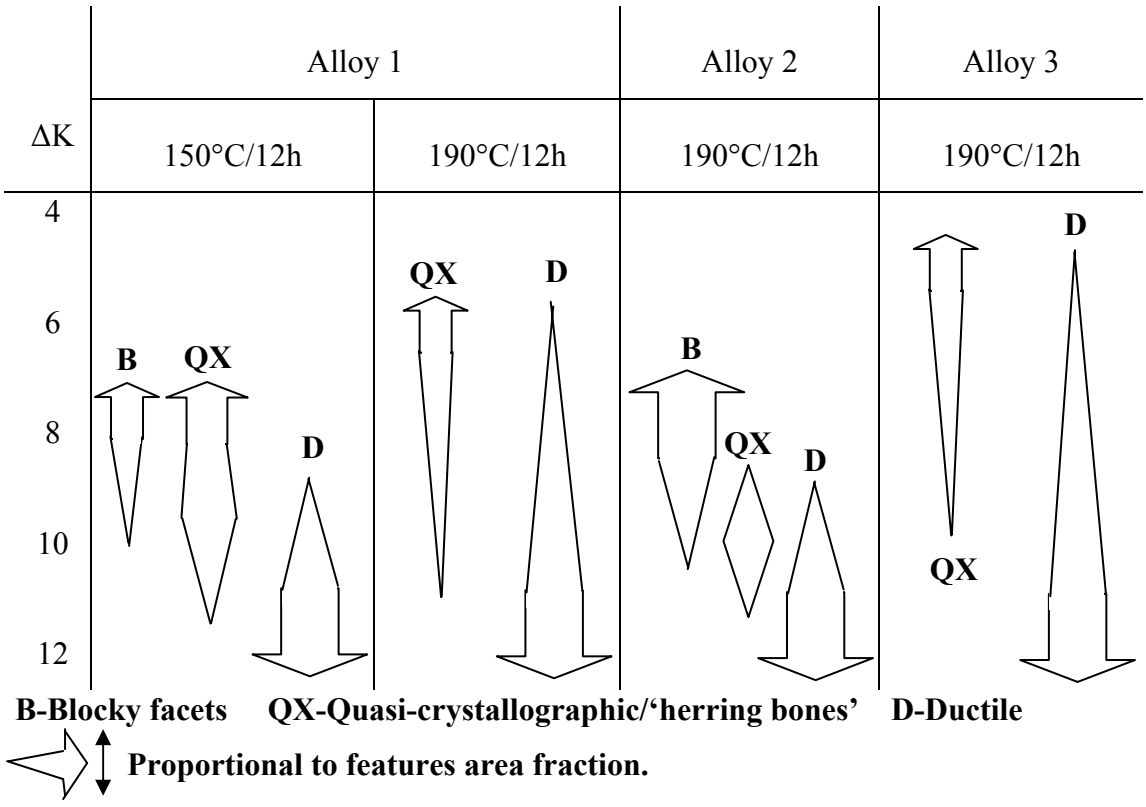

Table 5. Semi-quantitative evaluation of the nature of the fatigue fracture surfaces.

Heat treatment	150°C/12h	190°C/12h		
Alloys	**1**	**1**	**2**	**3**
Time integrated heat flow (precursors)	4.85	0.24	0.41	0.38
V_f (precursors) (%)	1.32	0.07	0.11	0.10
Average radius (precursors) (nm)	2.25	2.25	2.25	2.25
Time integrated heat flow (S phase)	2	15.36	15.1	17.4
V_f (S phase) (%)	0.54	4.18	4.11	4.74
Average radius (S phase) (nm)	20	20	20	20

Table 6. Precipitates size and estimated volume fraction for S phase and precipitate precursors.

Heat treatment	150°C/12h	190°C/12h		
Alloys	**1**	**1**	**2**	**3**
$\sqrt{V_f r_p}$ (x10^{-5})	2.97	0.15	0.25	0.23
L_{GS} (μm)*	24	24	196	22
N_c (x1e-1)	1.3	0.3	3.1	0.3

* $L_{GS} = \frac{\sum_{al\lg rain} A_{grain} \cdot d_{grain}}{A_{average} \cdot N}$ where A_{grain} and d_{grain} are respectively the area and diameter of each grain (as measured by hkl channel 5 software on EBSD maps), $A_{average}$ is the average area of the grains and N is the number of grains.

Table 7. Eq. 2 parameters and propensity for slip band formation criterion N_c.

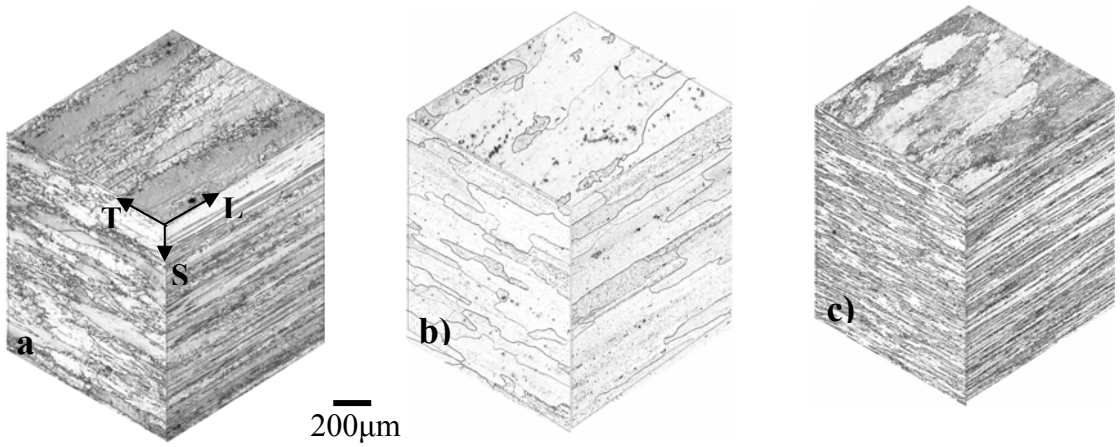

Fig 1. Optical micrographs of polished and etched sections of a) Alloy 1, b) Alloy 2 and c) Alloy 3.

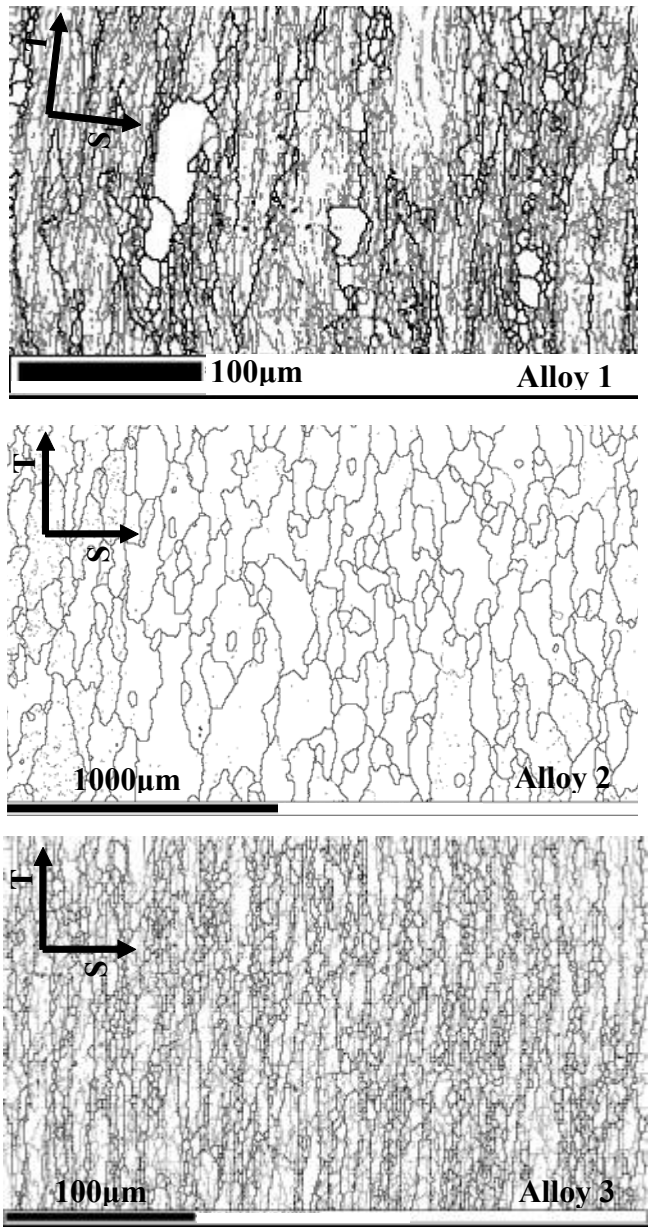

Fig. 2. EBSD grain boundary maps.

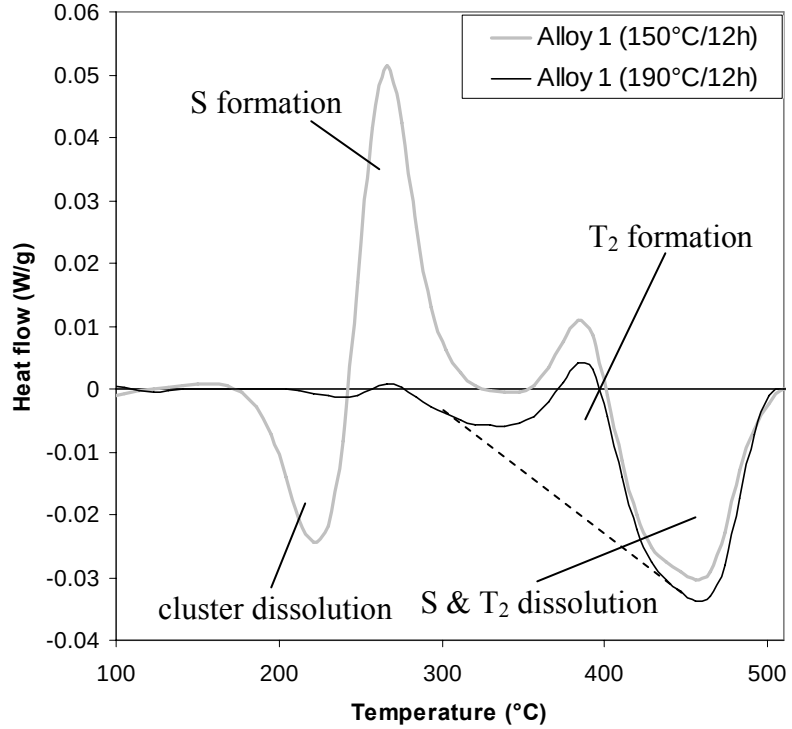

Fig. 3. DSC curve of Alloy 1 aged at 150°C and 190°C for 12h.

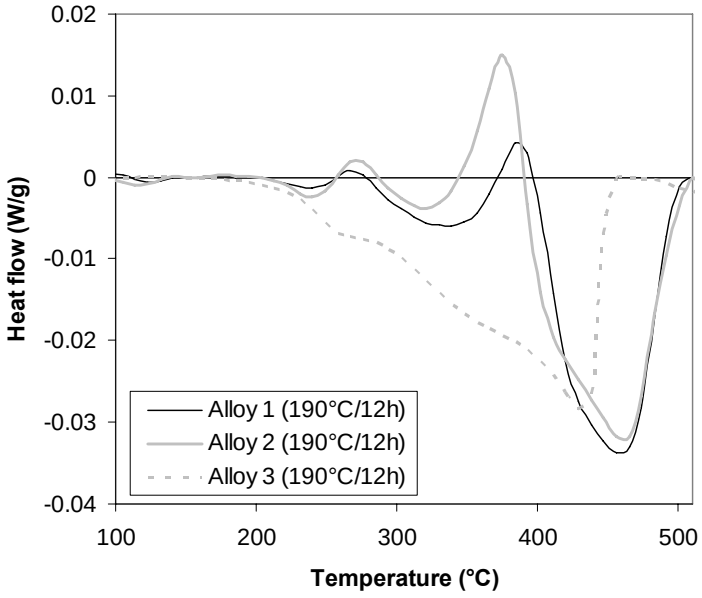

Fig. 4. DSC curve of Alloy 1, 2 and 3 aged at 190°C for 12h.

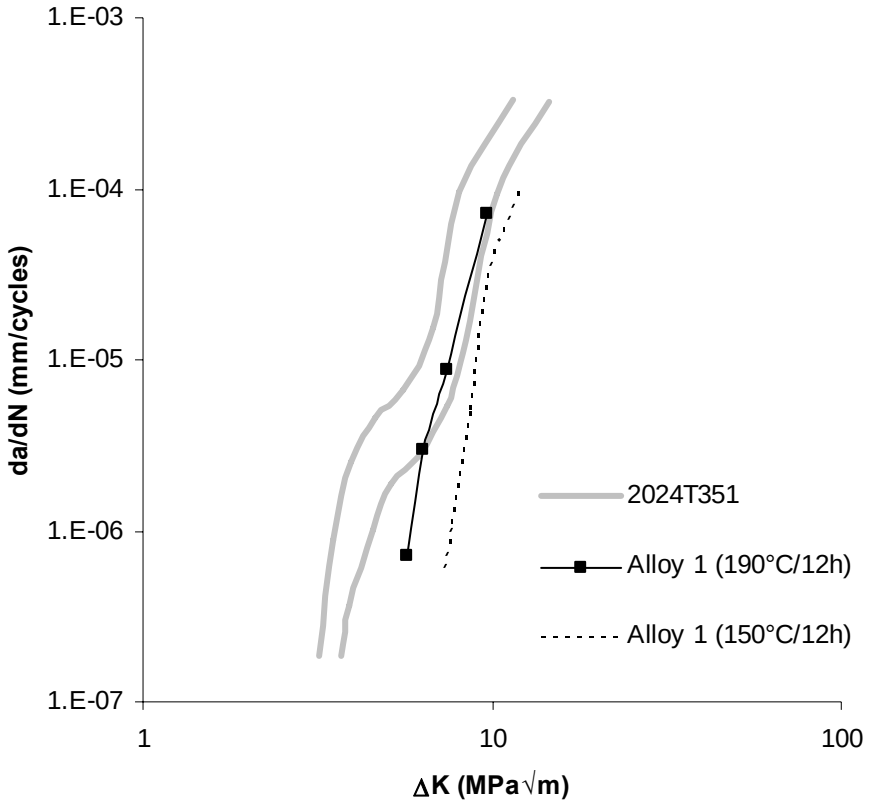

Fig. 5. Fatigue crack growth rate vs ΔK for Alloy 1 aged at 150°C and 190°C for 12h.

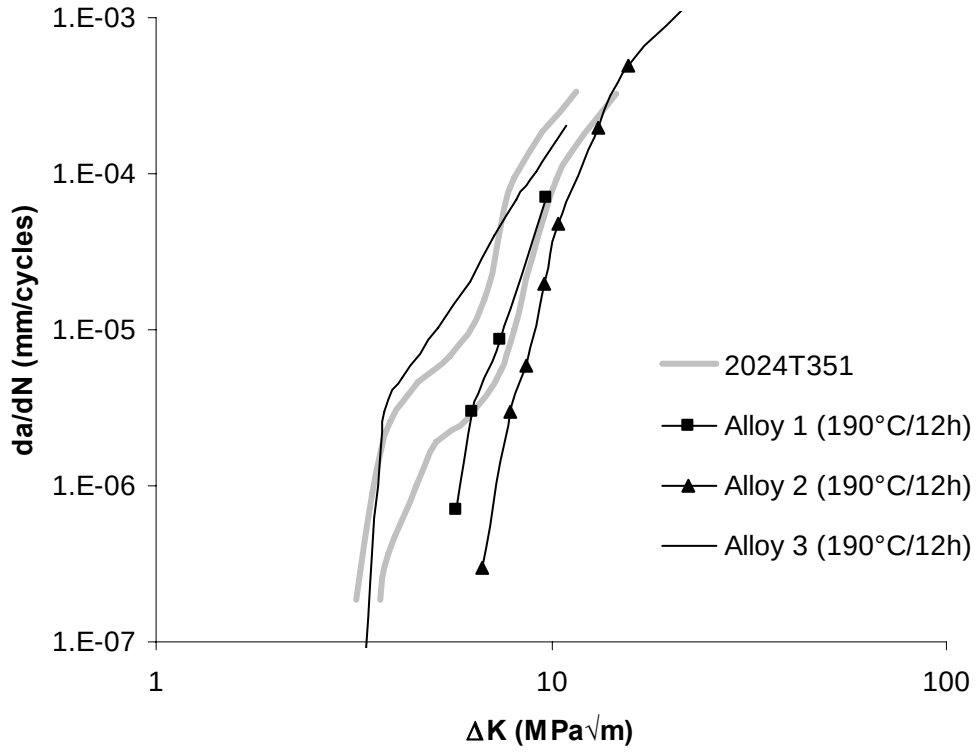

Fig. 6. Fatigue crack growth rate vs ΔK for Alloy 1,2 and 3 aged at 190°C for 12h.

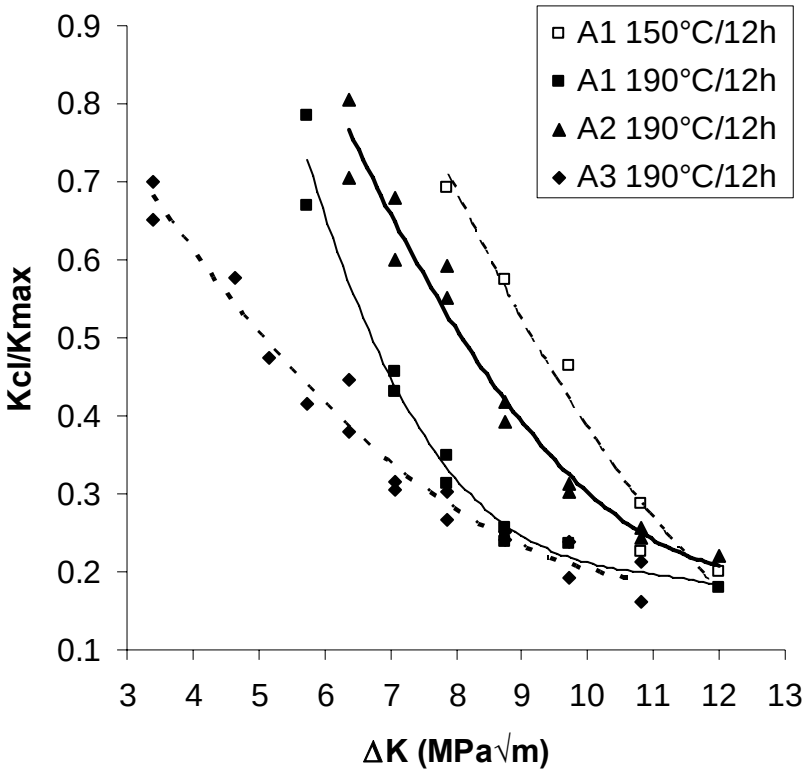

Fig. 7. Crack closure level vs ΔK for Alloy 1, 2 and 3 aged at 190°C for 12h and Alloy 1 aged at 150°C for 12h.

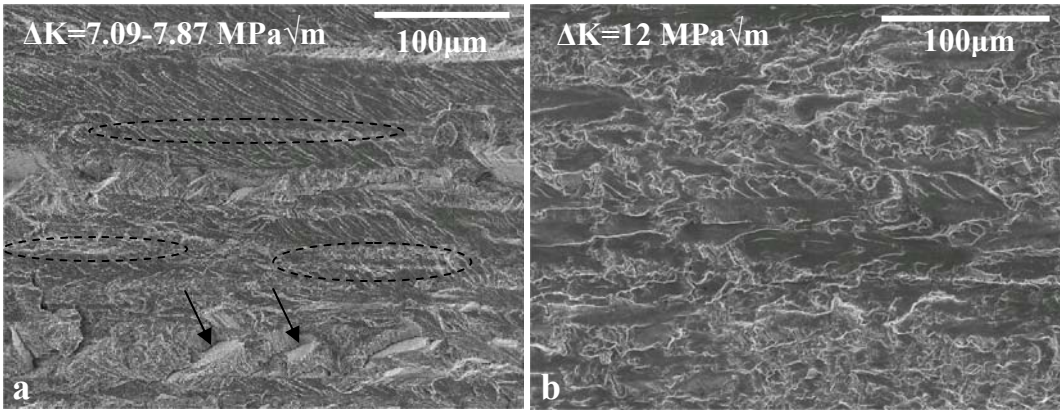

Fig. 8. SEM micrograph of fatigue fracture surfaces at mid-thickness for Alloy 1 aged at 150°C for 12h at (a) low ΔK (b) high ΔK. Linear features circled. Arrows indicates crystallographic features.

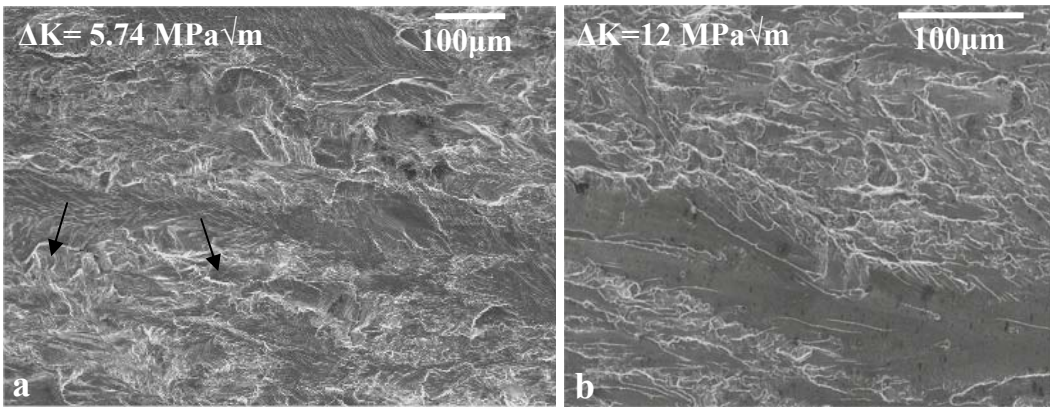

Fig. 9. SEM micrograph of fatigue fracture surfaces at mid-thickness for Alloy 1 aged at 190°C for 12h at (a) low ΔK (b) high ΔK. Arrows indicates crystallographic features.

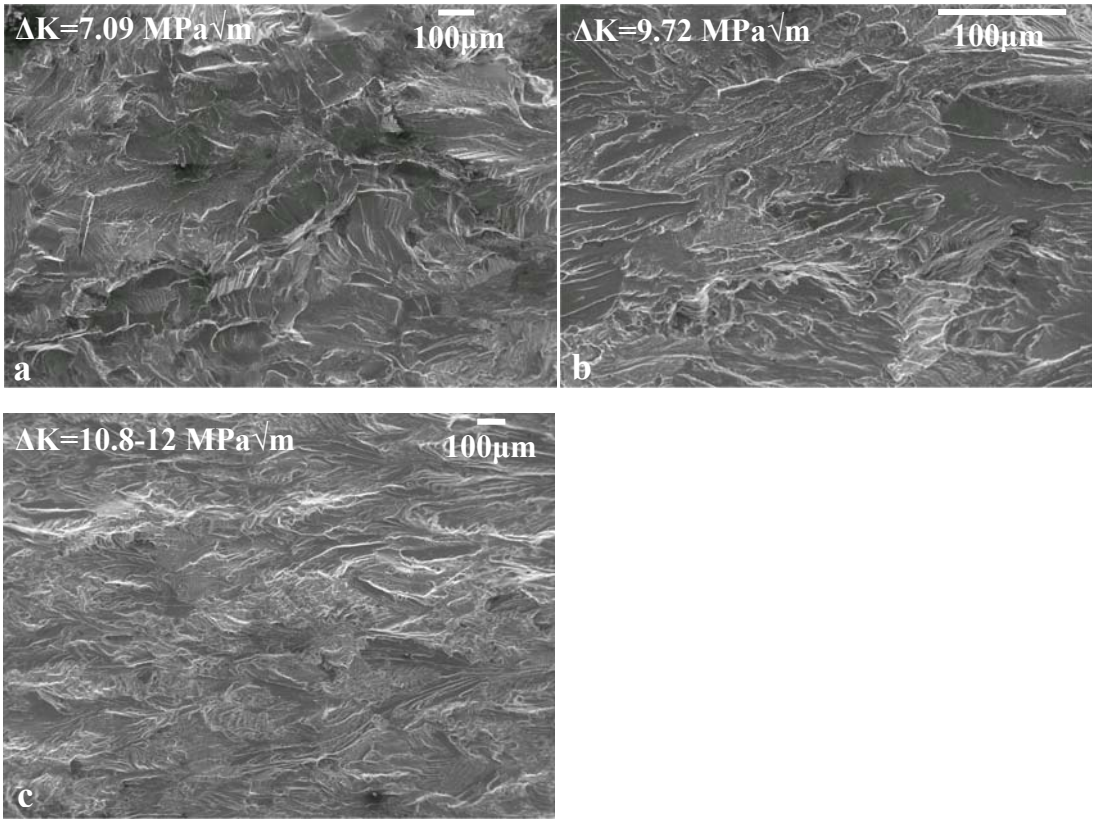

Fig. 10. SEM micrograph of fatigue fracture surfaces at mid-thickness for Alloy 2 aged at 190°C for 12h at (a) low ΔK (b) intermediate ΔK and (c) high ΔK.

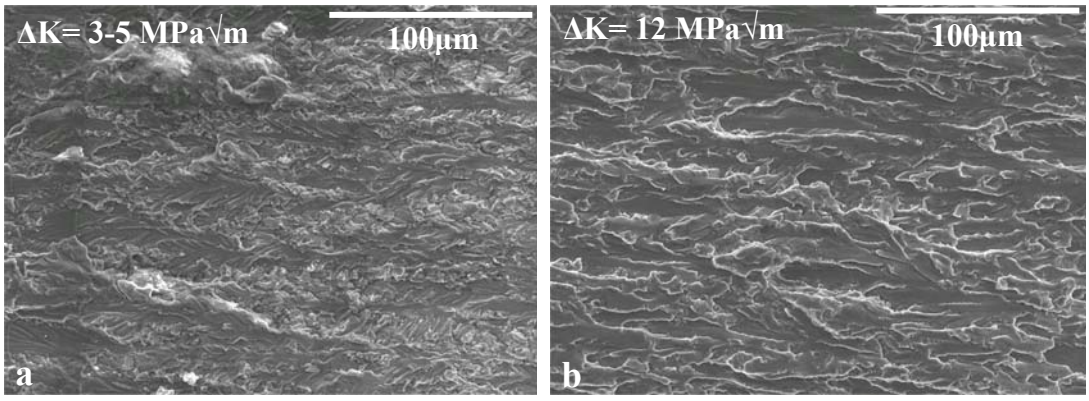

Fig. 11. SEM micrograph of fatigue fracture surfaces at mid-thickness for Alloy 3 aged at 190°C for 12h at (a) low ΔK (b) high ΔK.

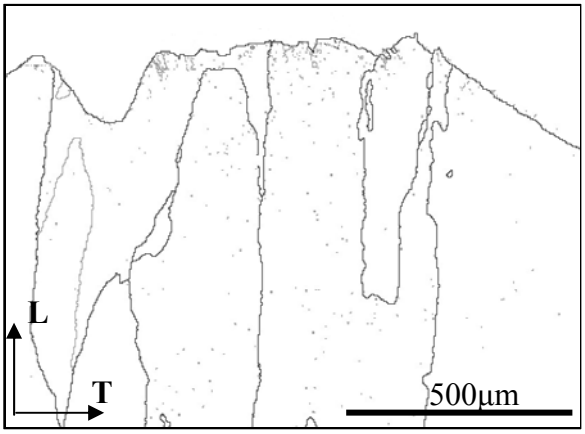

Fig. 12. EBSD map of Alloy 2 crack profile at low ΔK.

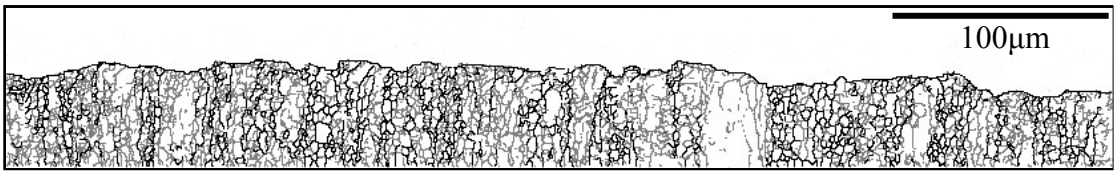

Fig. 13. EBSD map of Alloy 3 crack profile at low ΔK (LT face).

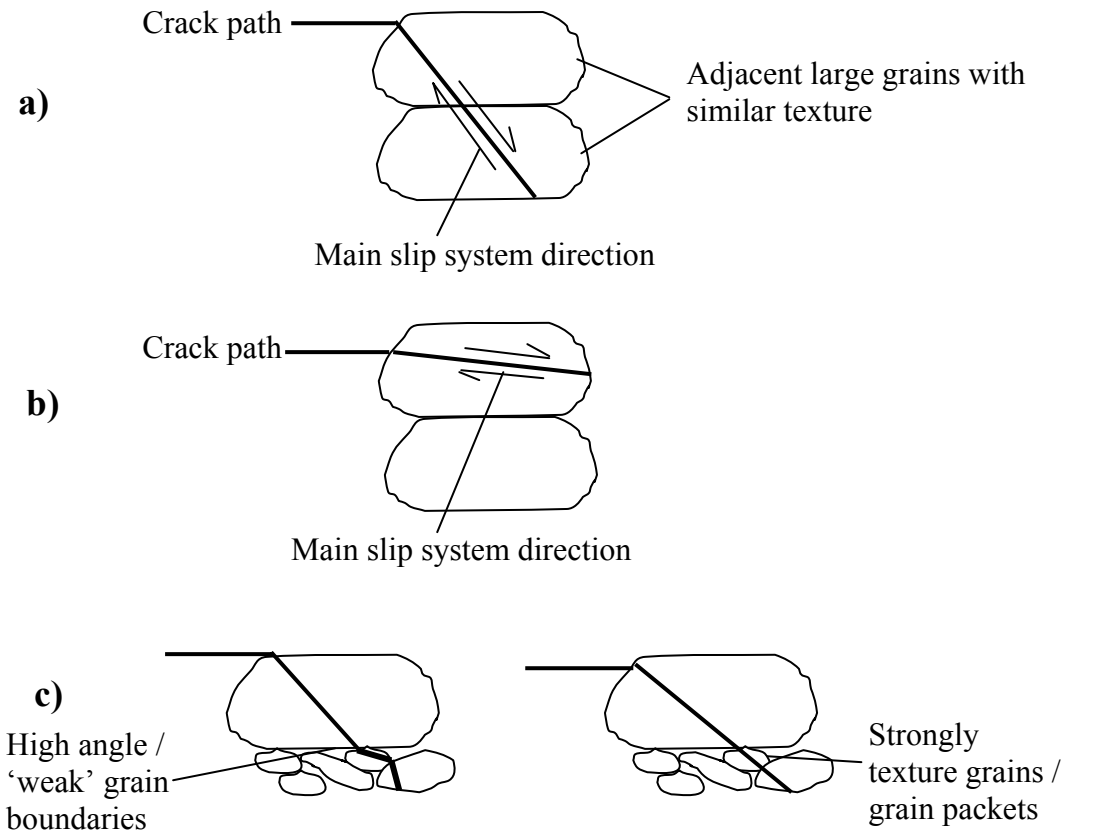

Fig. 14. Schematic drawing of adjacent grain interactions a) large deflection, faceted fracture surface, b) small/no deflection, flat fracture surface and c) small to large deflection, varied fracture surface features.

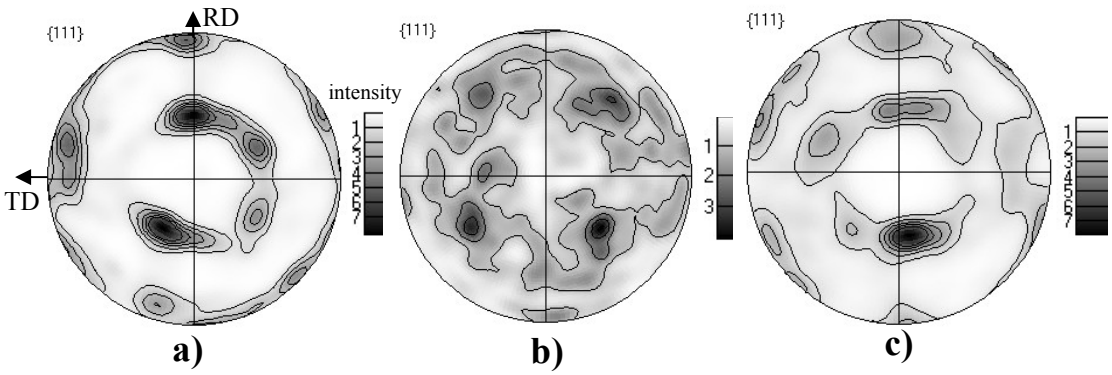

Fig. 15. {111}pole figures for a) Alloy 1, b) Alloy 2 and c) Alloy 3.